1 **Enhanced Natural Releases of Mercury in Response to Reduction of**

2 **Anthropogenic Emissions during the COVID-19 Lockdown by**

3 **Explainable Machine Learning**

4

5 Xiaofei Qin[1], Shengqian Zhou[1], Hao Li[1], Guochen Wang[1], Cheng Chen[1], Chengfeng Liu[1], Xiaohao

6 Wang[2], Juntao Huo[2], Yanfen Lin[2], Jia Chen[2], Qingyan Fu[2], Yusen Duan[2], Kan Huang[1,3,4*], Congrui

7 Deng[1*]

8 [1]Center for Atmospheric Chemistry Study, Shanghai Key Laboratory of Atmospheric Particle

9 Pollution and Prevention (LAP[3]), Department of Environmental Science and Engineering, Fudan

10 University, Shanghai, 200433, China

11 [2]State Ecologic Environmental Scientific Observation and Research Station for Dianshan Lake,

12 Shanghai Environmental Monitoring Center, Shanghai, 200030, China

13 [3]Institute of Eco-Chongming (IEC), Shanghai, 202162, China

14 [4]IRDR ICoE on Risk Interconnectivity and Governance on Weather/Climate Extremes Impact and

15 Public Health, Fudan University, Shanghai 200433, China

16 **Corresponding authors:** huangkan@fudan.edu.cn; congruideng@fudan.edu.cn

17

18 **Abstract.** The widespread of coronavirus (COVID-19) has significantly impacted the global human

19 activities. Compared to numerous studies on conventional air pollutants, atmospheric mercury that

20 has matched sources from both anthropogenic and natural emissions is rarely investigated. At a

21 regional site in Eastern China, an intensive measurement was performed, showing obvious

22 decreases of gaseous elemental mercury (GEM) during the COVID-19 lockdown, while not as

23 significant as the other air pollutants. Before the lockdown when anthropogenic emissions

24 dominated, GEM showed no correlation with temperature and negative correlations with wind speed

25 and the height of boundary layer. In contrast, GEM showed significant correlation with temperature

26 while the relationship between GEM and wind speed/boundary layer disappeared during the

27 lockdown, suggesting the enhanced natural emissions of mercury. By applying a machine learning

28 model and the Shapley Additive ExPlanation Approach, it was found that the mercury pollution

29   episodes before the lockdown were driven by anthropogenic sources, while they were mainly driven

30   by natural sources during and after the lockdown. Source apportionment results showed that the

31   absolute contribution of natural surface emissions to GEM unexpectedly increased (44%) during

32   the lockdown. Throughout the whole study period, a significant negative correlation was observed

33   between the absolute contribution of natural and anthropogenic sources to GEM. We conclude that

34   natural release of mercury could be stimulated to compensate the significantly reduced

35   anthropogenic GEM via the surface - air exchange balance of mercury.

36   **Keywords:** gaseous elemental mercury, lockdown, correlation, explainable machine learning,

37   natural mercury

38

39

40   **1 Introduction**

41   Mercury pollution has received widespread attention due to its long-range transport,

42   bioaccumulation, and neurotoxicity (Giang and Selin, 2016; Horowitz et al., 2017; Driscoll et al.,

43   2013). The atmosphere is the key to the distribution of mercury on the global scale, because gaseous

44   elemental mercury (the predominant form of mercury in the atmosphere, >90%) has relatively high

45   stability and long residence time, and can be transported through the atmosphere for long distances

46   (Xu et al., 2017; Mao et al., 2016). Mercury in the atmosphere derived from both anthropogenic

47   emissions and natural processes. The main anthropogenic sources of atmospheric mercury included

48   coal combustion, nonferrous smelters, cement production, waste incineration, and mining (Wu et

49   al., 2018; Wu et al., 2016). The amount of mercury in the atmosphere directly emitted by

50   anthropogenic activities accounted for about 30% of global mercury emissions (Streets et al., 2017;

51   Pacyna et al., 2010) and China was the country with the largest anthropogenic atmospheric mercury

52   emissions in the world (Hui et al., 2017). The natural sources of mercury in the atmosphere were

53   mainly from the exchange processes between natural surfaces (e.g., soil, vegetation, and water) and

54   the atmosphere (Gustin et al., 2008). Unlike anthropogenic emissions, natural releases of mercury

55   were passive emissions and were susceptible to various environmental factors, such as

56   meteorological parameters (e.g., solar radiation, temperature, and atmospheric turbulence), surface

57   properties (e.g., soil/water mercury content, organic matter, and microbial activity), and ambient air

58   characteristics (e.g., Hg^0 concentration and O_3 concentration in the atmosphere) (Zhu et al., 2016).

59   Previous studies have focused on the effects of various meteorological factors and different medium

60   properties on natural surface releases of mercury. The soil Hg^0 flux and solar radiation showed a

61   high positive correlation, which was generally considered that high solar radiation tended to

62   promote the reduction of Hg^{II} to Hg^0 (Carpi and Lindberg, 1997; Poissant et al., 2004; Bahlmann et

63   al., 2006). High wind speed was conductive to the release of mercury from seawater (Wanninkhof,

64   2014). The terrestrial vegetations acted as a global mercury pump (Jiskra et al., 2018) and

65   deforestation would increase forest floor radiation and temperature, thereby increasing Hg^0

66   emissions (Carpi et al., 2014; Mazur et al., 2014). However, few studies have investigated the impact

67   of changes in ambient GEM concentration in response to the natural surface emissions of Hg^0. Under

68   the background that the global Hg^0 concentration has been decreasing year by year (Zhang et al.,

69   2016b), it is particularly urgent and important to conduct such research.

70   China has taken many stringent and ambitious control measures since 2013 to tackle the severe air

71   pollution, such as imposing ultra-low emission standards on coal-fired power plants, and phasing

72   out small and high-emission factories (Zheng et al., 2018), These pollution control measures co-

73   benefited the significant reduction of anthropogenic mercury emissions (Wen et al., 2020; Liu et al.,

74   2018), The anthropogenic atmospheric mercury emissions of China fell by 22% from 2013 to 2017

75   (Liu et al., 2019) and correspondingly, decreasing trends in the annual mean atmospheric mercury

76   concentration were observed at both Chinese urban and remote sites (Qin et al., 2020; Tang et al.,

77   2018; Yin et al., 2018). In this regard, this change could be likely to affect the surface – air exchange

78   balance of mercury. In the early 2020, China's lockdown measures to control the spread of the 2019

79   Novel Coronavirus (COVID-19) resulted in a significant reduction in the emissions of primary air

80   pollutants (Chang et al., 2020). One study in the Beijing – Tianjin – Hebei region showed that the

81   anthropogenic emission of atmospheric mercury reduced by about 22% during the lockdown

82   compared with that before the lockdown (Wu et al., 2021). Therefore, the COVID-19 lockdown

83   provided a natural experiment to explore how the natural surface emissions of mercury would

84   respond to the dramatic reduction of anthropogenic mercury emissions. Traditionally, chemical

85   transport models were the most widely used tools for disentangling the contributions from

86   meteorology and various emission sources, while the performance of these models relied heavily on

87   the availability of updated emission inventories with high accuracy (Selin et al., 2007; Holmes et

88   al., 2010; Huang and Zhang, 2021). Therefore, applying traditional models to reproduce and explain

89   some special events and processes of atmospheric mercury could be limited by certain uncertainties.

90   Recently, data-driven methods such as machine learning has been widely used in atmospheric

91   science research (Grange et al., 2018; Vu et al., 2019; Qi et al., 2019). The model performance of

92   machine learning in predicting atmospheric pollutants (such as $PM_{2.5}$) was generally better than

93   traditional chemical transport models (Hou et al., 2022; Yang et al., 2021), however, these results

94   were less robust in terms of interpretability due to the "black box" nature of machine learning model.

95   With the development of data analysis methods, tools that can unlock the mystery of machine

96   learning has been emerging, such as the SHapley Additive exPlanation (SHAP) approach (Stirnberg

97   et al., 2021). Therefore, combined with new interpretation methods, machine learning can be a

98   promising alternative to study the behavior of pollutants in the atmosphere. However, few studies

99   have applied machine learning to the study of atmospheric mercury.

100   In this study, we first compared the concentration of GEM and its relationship with environmental

101   factors before, during, and after the COVID-19 lockdown. Observational evidence on the changes

102   of anthropogenic and natural sources of GEM was revealed. Then the drivers of the GEM variation

103   throughout the study period were explored by using the machine learning model and explained by

104   a game theoretic approach. Finally, we applied a receptor model to quantify the contribution of

105   anthropogenic and natural sources to GEM and unveiled the response of natural releases of mercury

106   to the reduction of anthropogenic mercury emissions.

107

108   **2 Materials and Methods**

109   **2.1 Site and Instrumentation**

110   Field measurements were conducted at the Dianshan Lake site (31.096°N, 120.988°E; 14 m a.g.l)

111   at the junction of Shanghai, Zhejiang, and Jiangsu provinces of the Yangtze River Delta (YRD)

112   region of China (Figure S1). It represents a rural setting and regional-scale air pollution

113   characteristics of the YRD region. A detailed description of the site can be found in our previous

114   works (Qin et al., 2019; Qin et al., 2020).

115   Ambient GEM concentration was measured by an automated mercury vapor analyzer (Tekran

116   2537B/1130/1135 system, Tekran Inc., Canada) at 5-min time resolution, more details of this

117   instrument can be found elsewhere (Qin et al., 2019). Water soluble ions in $PM_{2.5}$ (SO_4^{2-}, NO_3^-,

118   NH_4^+, Cl^-, Na^+, K^+, Mg^{2+}, and Ca^{2+}) and water soluble gases (NH_3 and SO_2) were continuously

119   measured by Monitor for AeRosols and Gases in ambient Air (MARGA) at a flow rate of 16.7 L/min

120   with a time resolution of 1 h (Wang et al., 2022b; Xu et al., 2020). Heavy metals in $PM_{2.5}$ (Pb, Fe,

121   Ba, Cr, Se, Cd, Ag, Ca, Mn, Cu, As, Ni, Zn, and V) were determined hourly by a multi-metal monitor

122   ($Xact^{TM}$ 625; Cooper Environmental, USA) (Wang et al., 2022a). Black carbon in $PM_{2.5}$ were

123   continuously measured by a multi-wavelength Aethalometer (AE-33, Magee Scientific, USA) (Li

124   et al., 2021). Organic carbon (OC) and elemental carbon (EC) in $PM_{2.5}$ were measured by an in situ

125   Semi-Continuous Organic Carbon and Elemental Carbon aerosol analyzer (RT-3195, Sunset

126   Laboratory, Beaverton, Oregon, USA) (Xu et al., 2018). SO_2, CO, O_3, and $PM_{2.5}$ were determined

127   by Thermo Fisher 43i, Thermo Fisher 48i-TLE, Thermo Fisher 49i, and Thermo Fisher 1405-F,

128   respectively. Meteorological parameters including air temperature, relative humidity, wind speed,

129   and wind direction were collected by using a series of Vaisala weather sensors (WXT530 Weather

130   Transmitter Series; Vaisala; Vantaa, Finland) with a time resolution of 10 min.

131   The air pollutants including CO, NO_2, and $PM_{2.5}$ at other ground monitoring stations in the YRD

132   region were obtained from the public database of China National Environmental Monitoring Centre.

133   The data of planetary boundary layer (PBL) height were obtained from the US National Oceanic

134   and Atmospheric Administration (https://www.ready.noaa.gov/archives.php, last access: 31

135   August, 2022). The 3-days air mass backward trajectories were calculated by applying the Hybrid

136   Single Particle Lagrangian Integrated Trajectory (HYSPLIT) model

137   (https://www.ready.noaa.gov/HYSPLIT.php, last access: 31 August, 2022), the MeteoInfo

138   software was used to perform cluster analysis of backward trajectories.

139

140   **2.2 Machine Learning Model**

141   The artificial neural network (ANN) model was used to simulate the GEM concentration at the DSL

142   site during the study period. Artificial neural network is a mathematical model based on the basic

143   principles of neural networks in biology. The network structure consists of input layer, hidden layer,

144   and output layer of neurons. The process of obtaining an ANN model is that the neurons of input

145   layer pass through each hidden layer and then reach the output layer. If the expected results are not

146   obtained in the output layer, the errors are propagated back and the neuron weights of each hidden

147   layer are iteratively updated to minimize them. In this study, long-term observational air pollutants

148   (SO_2, CO, O_3, NO_2, and $PM_{2.5}$) and meteorological data (air temperature, relative humidity, and

149   wind speed) in Shanghai (from March 1, 2015 to February 28, 2019) were chosen as input variables

150   for training. These variables were directly or indirectly related to the emissions (both anthropogenic

151   and natural sources), transport, and removal processes of GEM. For example, the main sources of

152   SO_2, CO, and NO_2 were fossil fuel combustions, which were also the largest anthropogenic sources

153   of GEM (Zhang et al., 2016a; Streets et al., 2011). The natural sources of GEM were mainly from

154   the release of land and sea surfaces, which were closely related to temperature, relative humidity,

155   and wind speed (Wang et al., 2014; Moore and Carpi, 2005). The detailed training and validation of

156   this model can be found in our previous study (Qin et al., 2022). Briefly, we have established an

157   ANN model through training the long-term observational data of GEM and other auxiliary

158   environmental parameters at DSL. The model performance has been satisfactorily verified by

159   multiple observational datasets in the YRD.

160

161   **2.3 Shapley Additive ExPlanation (SHAP) Approach**

162   The SHAP approach was applied in this study to explain the ANN model simulation results. This

163   approach constructs a distribution scheme based on coalitional game theory that comprehensively

164   considers the requirements of the conflicting parties, so as to ensure the fairness of the distribution

165   (Lundberg et al., 2018; Lundberg et al., 2020; Hou et al., 2022). In the game theory, the Shapley

166   value of a player represents the average contribution of the player in a cooperative game, which is

167   a fair distribution of the total gain generated by individual players (Lundberg and Lee, 2017b). In

168   the context of machine learning prediction, the Shapley value of a feature at a query point represents

169   the contribution of that feature to the prediction (response for regression or score of each class for

170   classification) at a particular query point (Aas et al., 2021). The Shapley value corresponds to the

171   deviation between the prediction for the query point and the average prediction caused by the feature,

172   and the sum of the Shapley values for all features for specific query point corresponds to the total

173   deviation of the prediction from the average (Kumar et al., 2020). The Shapley value of the ith

174   feature for the query point x is defined by the value function v:

175
$$\varphi_i(v_x) = \frac{1}{N}\sum_{S \subseteq \omega\backslash\{i\}} \frac{\frac{v_x(S \cup \{i\}) - v_x(S)}{(N-1)!}}{|S|!(N-|S|-1)!} \qquad (1)$$

176 Where N is the number of all features, ω is the set of all features, $|S|$ is the cardinality of the set

177 S, or the number of elements in the set S, v_x is the value function of the features in a set S for the

178 query point x. The value of the function indicates the expected contribution of the features in S to

179 the prediction for the query point x.

180

181 **2.4 Positive Matrix Factorization (PMF)**

182 The PMF model has proven to be a useful tool for obtaining source profiles and quantifying source

183 contributions of complex air pollution (Gibson et al., 2015). The basic principle of PMF is that the

184 concentration of the sample is determined by the source profiles with different contributions, which

185 can be described as follows.

186
$$X_{ij} = \sum_{k=1}^{P} g_{ik} f_{kj} + e_{ij} \qquad (2)$$

187 where X_{ij} represents the concentration of the jth species in the ith sample, g_{ik} is the contribution of

188 the kth factor in the ith sample, f_{kj} provides the information about the mass fraction of the jth species

189 in the kth factor, e_{ij} is the residual for specific measurement, and P represents the number of factors.

190 Detail description can be seen in previous studies (Qin et al., 2020; Qin et al., 2019).

191

192 **3 Results and Discussion**

193 **3.1 Changes in GEM Concentrations during the Lockdown**

194 Figure 1 shows the time series of hourly GEM concentrations during 1 January to 26 February, 2020.

195 Three periods were defined, i.e., 1 January to 23 January before the lockdown, 24 January to 14

196 February during the lockdown, and 15 February to 26 February after the lockdown. Before the

197 lockdown, hourly GEM showed strong fluctuations with frequent extreme concentrations higher

198 than 5 ng/m^3. In contrast, the diurnal variation of GEM was significantly weakened with hourly

199 concentrations all lower than 4 ng/m^3 during the lockdown. After the lockdown, GEM slightly

200 rebounded. On average, GEM declined sharply from 2.78 ng/m^3 before the lockdown to 2.06 ng/m^3

201 during the lockdown, and then rose slightly to 2.26 ng/m^3 after the lockdown. Figure 1 also shows

202 typical gaseous pollutants such as sulfur dioxide (SO$_2$), nitrogen dioxide (NO$_2$), and carbon

203 monoxide (CO) behaved similarly as GEM, as well as for PM$_{2.5}$ and its components such as black

204   carbon (BC), elemental carbon (EC), lead (Pb), and arsenic (As). This temporal pattern was expected,

205   as the nationwide reduction of automotive mobility and energy consumption due to the COVID-19

206   lockdown would certainly lead to drops in primary pollutants emissions. As shown in Figure S2, the

207   levels of CO, NO_2, and $PM_{2.5}$ in the Yangtze River Delta (YRD) declined sharply during the

208   lockdown by 26%, 61%, and 27%, respectively, which was consistent with emissions estimates

209   based on up-to-date activity levels in eastern China (Huang et al., 2021). For anthropogenic Hg

210   emissions, one study in the Beijing – Tianjin – Hebei region estimated a decline of approximate 22%

211   during the lockdown, which was mainly due to the reduction of cement clinker production, coal-

212   fired power plants, and residential coal combustion (Wu et al., 2021). We compared the

213   meteorological factors (including air temperature, wind speed, relative humidity, and planetary

214   boundary layer height) before, during, and after the lockdown (Figure 1). No significant changes of

215   the meteorological factors were observed before and during the lockdown. In addition, the 3-days

216   backward trajectory cluster analysis indicated that the transport patterns differed little between these

217   two periods (Figure S3). This suggested that the significant decline in GEM concentrations during

218   the lockdown was mainly due to the reduced mercury emissions, rather than changes of synoptic

219   conditions.

220
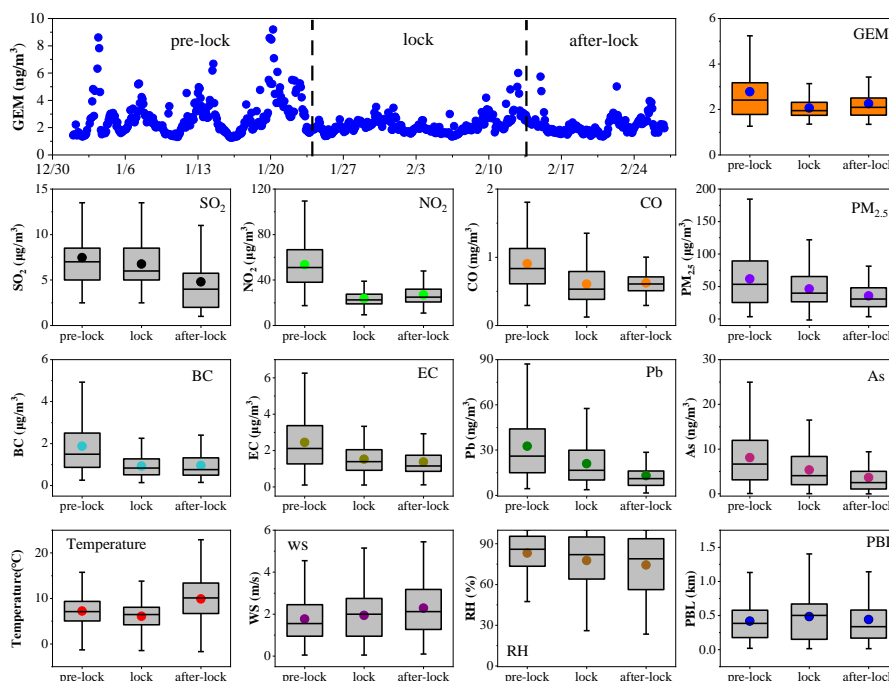
Figure 1. Hourly variations of GEM concentrations from 1 January to 26 February, 2020. Box

plots of GEM, SO_2, NO_2, CO, $PM_{2.5}$, BC, EC, Pb, As, and meteorological parameters

(temperature, wind speed, relative humidity, and planetary boundary layer height) before, during,

and after the lockdown are also shown.

3.2 Observational Evidences of Enhanced Effects of Natural Sources on GEM

Figure S4 further shows the reduction rates of GEM, SO_2, NO_2, CO, EC, Pb, As, and BC during the

lockdown were 26%, 9%, 56%, 33%, 38%, 36%, 34%, and 51%, respectively, compared to pre-lock.

Except for SO_2, GEM presented lower reduction rate than the other air pollutants, probably

suggesting the different release mechanism of GEM from the other air pollutants. In order to probe

the dynamic variation of GEM sources across the observational period, we first investigated the

correlations among GEM and main components of $PM_{2.5}$ and gaseous pollutants (Figure 2a). GEM

was found significantly correlated with the primary air pollutants such as CO, K^+, BC, and EC with

the correlation coefficients (*R*) above 0.7. This suggested that the main anthropogenic sources of

GEM were fossil fuel combustion and biomass burning in Shanghai, which was consistent with the

237 previous studies in the Yangtze River Delta (Qin et al., 2019; Tang et al., 2018).

238   BC, as a common product from fuel combustion, was used as a proxy for anthropogenic

239 emissions. In order to explore the changes in the sources of GEM, we further investigated the

240 relationship between GEM and BC before, during, and after the lockdown. As shown in Figure 2b-

241 d, R between GEM and BC before, during, and after the lockdown was 0.75, 0.69, and 0.73,

242 respectively. The R value during the lockdown was lower than of that before and after lockdown,

243 suggesting the influence of anthropogenic sources on GEM was weakened during the lockdown.

244 Different from BC that only derived from anthropogenic sources, GEM had additional natural

245 sources such as surface emission and ocean release (Obrist et al., 2018). Hence, the ratio of GEM/BC

246 can be simply applied as an indicator to reveal the relative importance of anthropogenic versus

247 natural sources. A higher GEM/BC ratio indicated the more importance of natural sources, and vice

248 versa. As shown in Figure 2e, the GEM/BC ratio significantly increased from 0.0019 before the

249 lockdown to 0.0032 during the lockdown, and then decreased slightly to 0.0028 after the lockdown.

250 This corroborated that the impact of natural sources on GEM could be more outstanding during the

251 lockdown than before and after the lockdown.
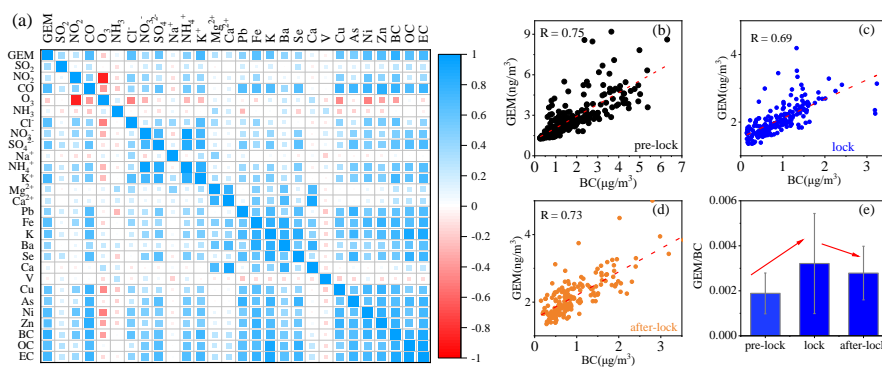
252

253 Figure 2. (a) Correlation coefficient matrix among GEM and $PM_{2.5}$ components and gaseous

254 pollutants during the whole study period. Relationship between GEM and BC (b) before, (c)

255 during, and (d) after the lockdown. (e) The change of GEM/BC ratios before, during, and after the
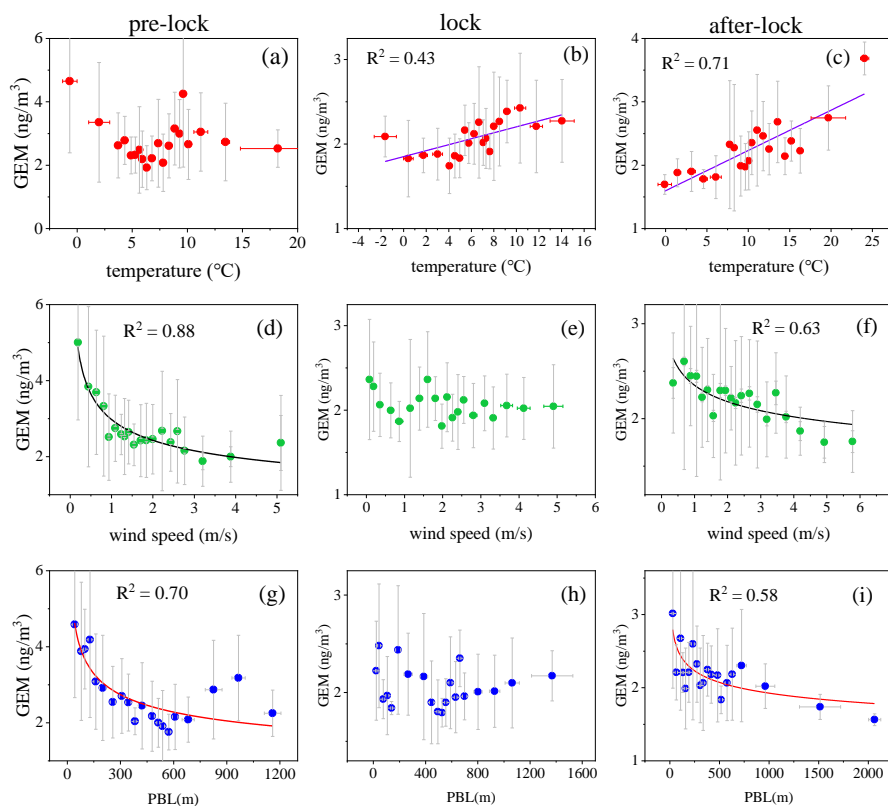
256 lockdown.

257

258   Previous studies have demonstrated the strong dependence of natural surface emissions on

259 meteorological factors such as temperature, wind speed, and relative humidity (Pannu et al., 2014;

260 Lindberg et al., 2007; Gustin et al., 2005). We compared the relationship between GEM and

261 meteorological parameters before, during, and after the lockdown to investigate the changes in

262 natural sources of mercury. As shown in Figure 3a-c, there was no clear correlation between GEM

263 and temperature before the lockdown while moderately high correlations during and after the

264 lockdown emerged with the correlation coefficients (R^2) of 0.43 and 0.71, respectively. This

265 indicated the enhanced role of natural sources on GEM concentrations due to the lockdown control

266 measures. For wind speed (Figure 3d-f), strongly negative correlations were observed with GEM

267 before and after the lockdown, but not during the lockdown. On the one hand, high wind speed was

268 beneficial to the diffusion of air pollutants in the atmosphere, which explained the negative

269 correlation between GEM and wind speed. On the other hand, high wind speed promoted the natural

270 surface release of mercury, partially canceling out the diffusion effect of wind speed, which induced

271 the ambiguous relationship between GEM and wind speed during the lockdown. The relationship

272 between GEM and PBL height was similar to that of wind speed, showing strongly negative

273 correlations before and after the lockdown while weak correlations during the lockdown (Figure 3g-

274 i). The increase of PBL height was beneficial to the diffusion of GEM. While the increase of PBL

275 height usually occurred in daytime when temperature was high, which was conducive to the natural

276 surface release of mercury. Therefore, ambient GEM did not decrease significantly with the increase

277 of PBL height during the lockdown.

278 Overall, all the observational evidences confirmed that the role of natural emissions on GEM

279 was more manifested due to the lockdown. However, all the results were based on qualitative data

280 analysis. In the following sections, the machine learning and source apportionment methods will be

281 applied to quantify the contribution of anthropogenic and natural sources to GEM during the three

282 defined periods.

Figure 3. Relationship between GEM concentration and (a-c) temperature, (d-f) wind speed, and (g-i) PBL height before, during, and after the lockdown.

3.3 Understanding the Drivers of GEM Variation by Explainable Machine Learning

We further conducted machine learning simulations using the trained artificial neural network (ANN), which has already been established by training the long-term (2015 - 2019) observational data of GEM and other necessary environmental parameters (including SO_2, NO_2, CO, O_3, $PM_{2.5}$, temperature, relative humidity, and wind speed) at the Dianshan Lake site (Qin et al., 2022). Figure 4a-b shows the comparison of ANN-simulated and observed GEM concentrations during the whole study period, and found they had good consistency ($R^2 = 0.67$). Then we applied the SHapley Additive exPlanation (SHAP) approach to uncover the mystery of the machine learning "black box" model (See methods in Section 2.3). This approach has the potential to quantify the global and local impacts of input features on model predictions (Lundberg and Lee, 2017a), which has been used in

297 various fields (Mangalathu et al., 2020; Hou et al., 2022; Lundberg et al., 2018; Zhong et al., 2021;

298 Wang et al., 2021).

299 We calculated the SHAP value of each feature to represent the global importance of the feature,

300 which can be used to indicate the general impact of various features across all samples. As shown

301 in Figure 4c, by comparing the average absolute SHAP values, $PM_{2.5}$ ranked as the most important

302 feature, which changed the simulated GEM concentrations by 0.30 ± 0.20 ng/m^3, followed by CO

303 and temperature with the SHAP values of 0.16 ± 0.25 and 0.14 ± 0.09 ng/m^3, respectively. The

304 average values of the remaining factors were less than 0.1 ng/m^3. We further investigated the

305 relationship between the SHAP value of each feature and its concentration. As shown in Figure 4c-

306 k, the higher concentrations of $PM_{2.5}$, CO, and SO_2 generally corresponded to the higher SHAP

307 values, which can be interpreted as the positive effect of various anthropogenic emission sources on

308 GEM. A similar relationship was also found for temperature and relative humidity, also suggesting

309 the positive influence of natural surface emissions on GEM. In contrast, the SHAP value of wind

310 speed negatively correlated with the magnitude of wind speed, indicating the

311 diffusion/accumulation effect of wind speed on GEM. The SHAP values of NO_2 and O_3 did not

312 show obvious correlations with their concentrations, indicating their negligible effects on regulating

313 the GEM variation.
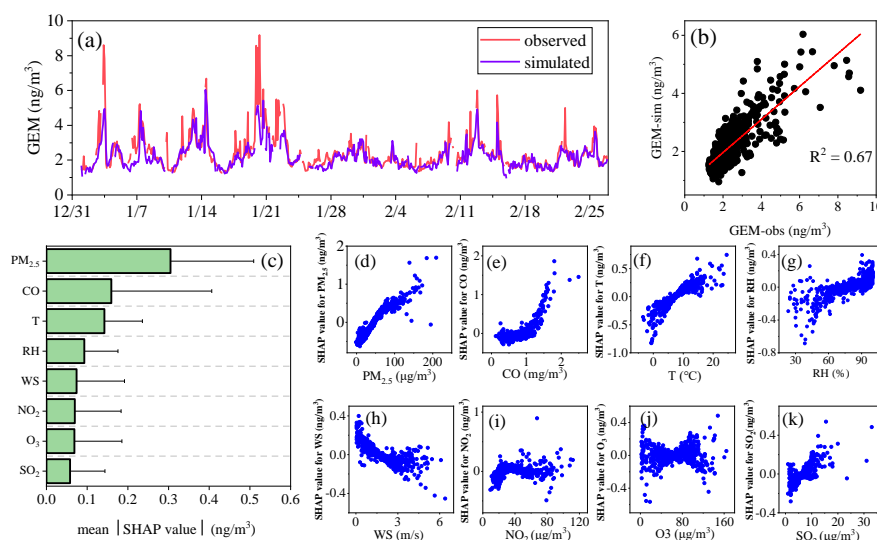
314

315 Figure 4. (a) Time-series of observed and ANN-simulated GEM concentrations during the study

316 period. (b) Linear correlation between observed and ANN-simulated GEM concentrations. (c) The

13

317   ranking of input features calculated via the SHAP algorithm (d-k) Relationship between SHAP

318   value and corresponding concentration of each feature.

319

320   To more explicitly identify the drivers to the dynamic variation of GEM, process analysis of

321 GEM pollution episodes was conducted. One pollution episode was defined as its average GEM

322 concentration more than 35% of the day before the episode and lasted for more than three days.

323 Based on this criterion, two pollution episodes (PE1 and PE2) before the lockdown, one pollution

324 episode (PE3) during the lockdown, and one pollution episode (PE4) after the lockdown were

325 selected (Figure S5). As shown in Figure 5, the drivers of the first two pollution episodes were

326 significantly different from the last two. The main influencing factors in PE1 were $PM_{2.5}$ and CO,

327 which represented anthropogenic sources, contributing 0.65 and 0.51 ng/m^3 to the GEM variation,

328 respectively. Similar to PE1, $PM_{2.5}$ and CO in PE2 contributed the most to the GEM variation of

329 0.35 and 0.12 ng/m^3, respectively. This indicated that the two mercury pollution episodes before the

330 lockdown were mainly driven by anthropogenic sources. In contrast, in PE3 and PE4, temperature

331 ranked the first among all the variables, with contribution to GEM of 0.10 and 0.14 ng/m^3,

332 respectively. This suggested that these two pollution episodes during and after the lockdown

333 occurred under the dominance of natural sources.

334   In addition, we found that there was a trade-off between the SHAP value of temperature and

335 the SHAP value of $PM_{2.5}$ and CO. As shown in Figure 5b-c, the SHAP value of temperature

336 decreased with the increase of the SHAP value of $PM_{2.5}$ and CO throughout the study period. This

337 probably suggested that the increase of anthropogenic GEM emissions may inhibit the release of

338 natural sources to some extents, which will be discussed later.

339

340
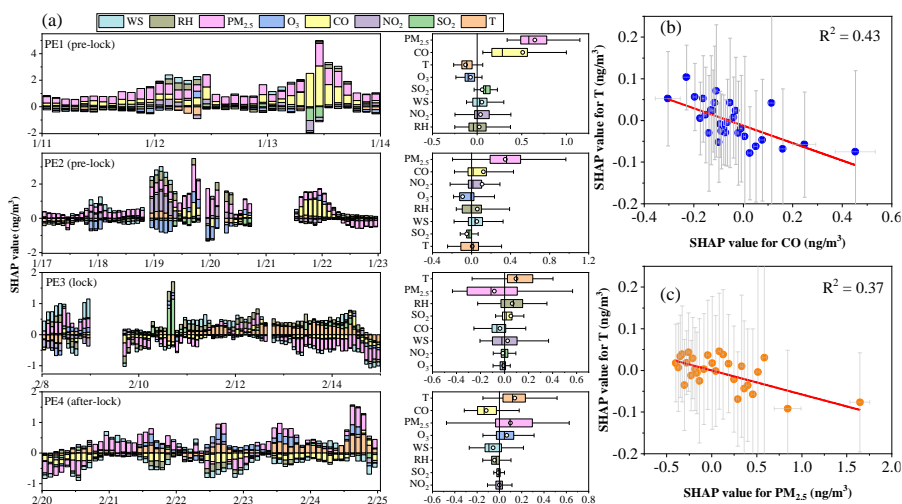
Figure 5. (a) Time series and box plots of each feature's SHAP value during the four mercury pollution episodes (b-c) Relationship between SHAP value of temperature and SHAP value of CO and PM$_{2.5}$ during the whole study period

3.4 Response of Natural Release of GEM to the Lockdown

To quantify the changes in the contribution of different sources to GEM, we applied the PMF model to analyze the sources of GEM during the whole study period. Figure S6 shows the resolved factors and factor loadings, which were similar to the results by previous study at the same site (Qin et al., 2020). A total of six sources were resolved, namely coal combustion with high loadings of SO$_4^{2-}$, Pb, K$^+$, As, and Se, natural surface emissions with high loadings of temperature and NH$_3$, vehicle emission with high loadings of NO, ship emission with high loading of Ni, iron and steel production with high loadings of Fe, Cr, and Mn, and cement production with high loading of Ca. The mean contributions of the six factors above to GEM were 55%, 28%, 7%, 5%, 3%, and 3%, respectively (Figure S6).

Figure 6a shows the time-series of apportioned GEM concentrations and relative contributions from six sources during three periods. Significant changes in the sources of GEM were observed due to the lockdown. The contribution of coal combustion fell from 60% before the lockdown to 51% during the lockdown and 48% after the lockdown. On the opposite, the relative contribution of

15

361 natural surface emissions rose significantly from 20% before the lockdown to 39% during the

362 lockdown, and then dropped slightly to 33% after the lockdown. In addition to the increased relative

363 contribution of natural surface emissions, its absolute contribution to GEM concentration increased

364 significantly from 0.55 ng/m^3 before the lockdown to 0.80 ng/m^3 during the lockdown, i.e., a 44%

365 increase (Figure 6b). Considering that the synoptic conditions varied little before and during the

366 lockdown, both increases in the absolute and relative contribution of natural surface emissions to

367 GEM during the lockdown should be stimulated by the significant reduction of anthropogenic

368 mercury emissions. Indeed, Figure 6c shows that the absolute contribution of natural surface

369 emissions to GEM and the contribution of anthropogenic sources exhibited a significant negative

370 correlation throughout the study period ($R^2 = 0.86$). This indicated that the significant reduction of

371 anthropogenic emissions would lead to a significant decrease in the GEM concentration, thereby

372 disrupting the exchange balance of mercury between the natural surfaces (including soil, vegetation,

373 and water bodies, etc.) and the atmosphere, resulting in an increase of natural surface release to

374 compensate for the decrease of GEM concentration in the atmosphere.

375
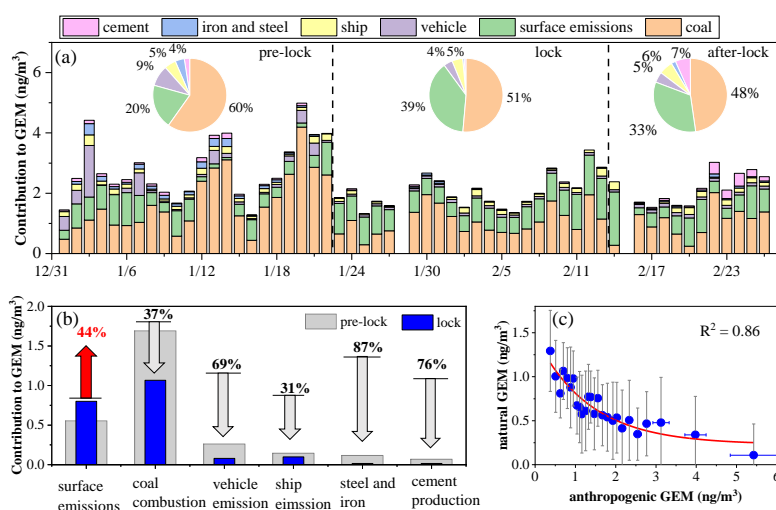
377 Figure 6. (a) Daily average concentrations of apportioned GEM from six sources based on PMF

378 modeling. Pie charts represent the relative contribution of the six sources to GEM during three

379 periods (b) Changes of absolute contribution of natural and anthropogenic sources to GEM before

380 and during the lockdown (c) Relationship between absolute contribution of natural surface

381   emissions and anthropogenic sources to GEM during the whole study period

382

383   **4 Conclusions and Implications**

384   In this work, we investigated the changes of the impact of anthropogenic and natural sources on

385   GEM in the suburbs of eastern China in the early 2020. Due to the COVID-19 lockdown, GEM was

386   significantly reduced by 0.72 ng/m^3 compared to that before the lockdown. However, the reduction

387   extent of GEM was not as strong as most of the other gaseous pollutants (NO_2 and CO) and primary

388   aerosol species (EC, BC, Pb, and As). Before the lockdown when anthropogenic emissions

389   dominated, GEM showed no correlation with temperature and negative correlations with wind speed

390   and the height of PBL. In contrast, GEM showed significant correlation with temperature while the

391   relationship between GEM and wind speed/PBL disappeared during the lockdown, suggesting the

392   enhanced natural emissions of mercury. By applying a machine learning model, GEM was well

393   simulated and the results were interpreted by the Shapley Additive ExPlanation Approach. It was

394   found that the mercury pollution episodes before the lockdown were driven by anthropogenic

395   sources, while they were mainly driven by natural sources during and after the lockdown. Source

396   apportionment results showed that the relative contribution of natural sources to GEM during the

397   lockdown reached 39%, which was significantly higher than that before the lockdown (20%). The

398   absolute contribution of natural sources to GEM during the lockdown was about 0.80 ng/m^3, 44%

399   higher than that before the lockdown. Finally, we revealed the negative correlation between the

400   absolute contribution of natural sources and anthropogenic sources, suggesting the natural release

401   of mercury could be enhanced in response to the significant reduction of anthropogenic mercury

402   emissions.

403   In the long-term, the surface ambient mercury concentration in the northern hemisphere decreased

404   by 30-40% from 1990 to 2010 (Slemr et al., 2011; Soerensen et al., 2012; Cole et al., 2014). From

405   2013 to 2017, the gaseous total mercury concentration in China decreased by about 12% (Liu et al.,

406   2019). It has been long recognized mitigation of anthropogenic mercury emissions regulated this

407   global or regional trend, while the role of natural mercury emissions is less known. Specifically, the

408   response of natural mercury release to the reduction of ambient Hg^0 concentration is ambiguous,

409   which limits better understanding the role of natural sources in global mercury cycling. In this study,

17

410   the COVID-19 lockdown provided a natural experiment on assessing the dynamic behavior of

411   natural and anthropogenic contributions to gaseous elementary mercury by different means. As

412   shown in Figure S7, the sum of the SHAP values of CO and $PM_{2.5}$ exhibited a good positive

413   correlation with the concentration of GEM contributed by anthropogenic sources based on PMF

414   modeling (R^2 = 0.72). Moderate correlation was also derived between the SHAP value of

415   temperature and the concentration of GEM contributed by natural sources ($R^2 = 0.50$). This indicated

416   that the results of machine learning with an explainable approach and the traditional receptor model

417   were consistent and corroborated each other. This study highlighted that machine learning coupled

418   with reliable interpretation methods can well quantify the role of different factors in the process of

419   air pollution, showing great potential in the fields of atmospheric science.

420   The natural release of mercury mainly comes from the exchange between the natural surfaces and

421   the atmosphere, including two processes: (1) the formation of volatile Hg^0 in the surface and (2) the

422   mass transfer of Hg^0 between the interfaces (Zhu et al., 2016). At locations with high ambient Hg^0

423   concentrations (e.g., mining areas and landfills), the exchange of mercury between the surface and

424   the atmosphere is always dominated by deposition, regardless changes in meteorological conditions

425   (Bash and Miller, 2007; Wang et al., 2007; Zhu et al., 2013). Fluctuations in ambient Hg^0

426   concentrations can change the Hg^0 concentration gradient at the interfaces and thus affect the Hg^0

427   exchange flux (Xin and Gustin, 2007). The results of this study imply that the declining in global

428   anthropogenic mercury emissions could stimulate increases in natural surface releases, which may

429   pose challenges to future control of atmospheric mercury pollution.

430

431   **Data Availability Statement**

432   All data has been uploaded to Zendo (https://doi.org/10.5281/zenodo.6654670).

433

434   **Author contributions**

435   XQ, CD, and KH designed this study. XQ and SZ performed measurements and data analysis.

436   XW, QF, JC, YL, YD, and JH performed data collection. XQ and KH wrote the paper.

437   All have commented on and reviewed the paper.

438

439   **Competing interests**

440   The authors declare that they have no conflict of interest.

441

442   **Acknowledgments**

443   This work was financially supported by the National Science Foundation of China (grant no.

444   42175119, 21777029, 91644105).

445

446   **References**

447   Aas, K., Jullum, M., and Loland, A.: Explaining individual predictions when features are dependent:

448   More accurate approximations to Shapley values, Artificial Intelligence, 298,

449   10.1016/j.artint.2021.103502, 2021.

450   Bahlmann, E., Ebinghaus, R., and Ruck, W.: Development and application of a laboratory flux

451   measurement system (LFMS) for the investigation of the kinetics of mercury emissions from soils,

452   Journal of Environmental Management, 81, 114-125, 10.1016/j.jenvman.2005.09.022, 2006.

453   Bash, J. O. and Miller, D. R.: A note on elevated total gaseous mercury concentrations downwind

454   from an agriculture field during tilling, Sci. Total Environ., 388, 379-388,

455   10.1016/j.scitotenv.2007.07.012, 2007.

456   Carpi, A. and Lindberg, S. E.: Sunlight-mediated emission of elemental mercury from soil amended

457   with municipal sewage sludge, Environmental science & technology, 31, 2085-2091, 10.1021/es960910+,

458   1997.

459   Carpi, A., Fostier, A. H., Orta, O. R., dos Santos, J. C., and Gittings, M.: Gaseous mercury emissions

460   from soil following forest loss and land use changes: Field experiments in the United States and Brazil,

461   Atmospheric Environment, 96, 423-429, 10.1016/j.atmosenv.2014.08.004, 2014.

462   Chang, Y., Huang, R. J., Ge, X., Huang, X., Hu, J., Duan, Y., Zou, Z., Liu, X., and Lehmann, M. F.:

463   Puzzling haze events in China during the coronavirus (COVID-19) shutdown, Geophys Res Lett,

464   e2020GL088533, 10.1029/2020GL088533, 2020.

465   Cole, A. S., Steffen, A., Eckley, C. S., Narayan, J., Pilote, M., Tordon, R., Graydon, J. A., St Louis,

466   V. L., Xu, X., and Branfireun, B. A.: A Survey of Mercury in Air and Precipitation across Canada: Patterns

467   and Trends, Atmosphere, 5, 635-668, 10.3390/atmos5030635, 2014.

468   Driscoll, C. T., Mason, R. P., Chan, H. M., Jacob, D. J., and Pirrone, N.: Mercury as a global

469   pollutant: sources, pathways, and effects, Environmental science & technology, 47, 4967-4983,

470   10.1021/es305071v, 2013.

471   Giang, A. and Selin, N. E.: Benefits of mercury controls for the United States, Proceedings of the

472   National Academy of Sciences of the United States of America, 113, 286-291, 10.1073/pnas.1514395113,

473   2016.

474   Gibson, M. D., Haelssig, J., Pierce, J. R., Parrington, M., Franklin, J. E., Hopper, J. T., Li, Z., and

475   Ward, T. J.: A comparison of four receptor models used to quantify the boreal wildfire smoke contribution

476   to surface $PM_{2.5}$ in Halifax, Nova Scotia during the BORTAS-B experiment, Atmos. Chem.

477   Phys., 15, 815-827, 10.5194/acp-15-815-2015, 2015.

478   Grange, S. K., Carslaw, D. C., Lewis, A. C., Boleti, E., and Hueglin, C.: Random forest

479   meteorological normalisation models for Swiss PM10 trend analysis, Atmos. Chem. Phys., 18, 6223-

480   6239, 10.5194/acp-18-6223-2018, 2018.

481   Gustin, M. S., Lindberg, S. E., and Weisberg, P. J.: An update on the natural sources and sinks of

482   atmospheric mercury, Appl. Geochem., 23, 482-493, 10.1016/j.apgeochem.2007.12.010, 2008.

483   Gustin, M. S., Engle, M., Ericksen, J., Xin, M., Krabbenhoft, D., Lindberg, S., Olund, S., and Rytuba,

484   J.: New insights into mercury exchange between air and substrate, Geochimica Et Cosmochimica Acta,

485   69, A700-A700, 2005.

486   Holmes, C. D., Jacob, D. J., Corbitt, E. S., Mao, J., Yang, X., Talbot, R., and Slemr, F.: Global

487   atmospheric model for mercury including oxidation by bromine atoms, Atmos. Chem. Phys., 10, 12037-

488   12057, 10.5194/acp-10-12037-2010, 2010.

489   Horowitz, H. M., Jacob, D. J., Zhang, Y., Dibble, T. S., Slemr, F., Amos, H. M., Schmidt, J. A.,

490   Corbitt, E. S., Marais, E. A., and Sunderland, E. M.: A new mechanism for atmospheric mercury redox

491   chemistry: implications for the global mercury budget, Atmospheric Chemistry and Physics, 17, 6353-

492   6371, 10.5194/acp-17-6353-2017, 2017.

493   Hou, L., Dai, Q., Song, C., Liu, B., Guo, F., Dai, T., Li, L., Liu, B., Bi, X., Zhang, Y., and Feng, Y.:

494   Revealing Drivers of Haze Pollution by Explainable Machine Learning, Environmental Science &

495   Technology Letters, 9, 112-119, 10.1021/acs.estlett.1c00865, 2022.

496   Huang, S. and Zhang, Y.: Interannual Variability of Air-Sea Exchange of Mercury in the Global

497   Ocean: The "Seesaw Effect" in the Equatorial Pacific and Contributions to the Atmosphere,

498   Environmental science & technology, 55, 7145-7156, 10.1021/acs.est.1c00691, 2021.

499   Huang, X., Ding, A., Gao, J., Zheng, B., Zhou, D., Qi, X., Tang, R., Wang, J., Ren, C., Nie, W., Chi,

500   X., Xu, Z., Chen, L., Li, Y., Che, F., Pang, N., Wang, H., Tong, D., Qin, W., Cheng, W., Liu, W., Fu, Q.,

501   Liu, B., Chai, F., Davis, S. J., Zhang, Q., and He, K.: Enhanced secondary pollution offset reduction of

502   primary emissions during COVID-19 lockdown in China, Natl Sci Rev, 8, nwaa137,

503   10.1093/nsr/nwaa137, 2021.

504   Hui, M. L., Wu, Q. R., Wang, S. X., Liang, S., Zhang, L., Wang, F. Y., Lenzen, M., Wang, Y. F., Xu,

505   L. X., Lin, Z. T., Yang, H., Lin, Y., Larssen, T., Xu, M., and Hao, J. M.: Mercury Flows in China and

506   Global Drivers, Environmental science & technology, 51, 222-231, 10.1021/acs.est.6b04094, 2017.

507   Jiskra, M., Sonke, J. E., Obrist, D., Bieser, J., Ebinghaus, R., Myhre, C. L., Pfaffhuber, K. A.,

508   Wangberg, I., Kyllonen, K., Worthy, D., Martin, L. G., Labuschagne, C., Mkololo, T., Ramonet, M.,

509   Magand, O., and Dommergue, A.: A vegetation control on seasonal variations in global atmospheric

510   mercury concentrations, Nat. Geosci., 11, 244-+, 10.1038/s41561-018-0078-8, 2018.

511   Kumar, I. E., Venkatasubramanian, S., Scheidegger, C., and Friedler, S. A.: Problems with Shapley-

512   value-based explanations as feature importance measures, International Conference on Machine

513   Learning (ICML), Electr Network, 2020

514   Jul 13-18, WOS:000683178505057, 2020.

515   Li, H., Huang, K., Fu, Q., Lin, Y., Chen, J., Deng, C., Tian, X., Tang, Q., Song, Q., and Wei, Z.:

516   Airborne black carbon variations during the COVID-19 lockdown in the Yangtze River Delta megacities

517   suggest actions to curb global warming, Environ Chem Lett, 1-10, 10.1007/s10311-021-01327-3, 2021.

518   Lindberg, S., Bullock, R., Ebinghaus, R., Engstrom, D., Feng, X. B., Fitzgerald, W., Pirrone, N.,

519   Prestbo, E., and Seigneur, C.: A synthesis of progress and uncertainties in attributing the sources of

520   mercury in deposition, Ambio, 36, 19-32, 2007.

521   Liu, K., Wang, S., Wu, Q., Wang, L., Ma, Q., Zhang, L., Li, G., Tian, H., Duan, L., and Hao, J.: A

522   Highly Resolved Mercury Emission Inventory of Chinese Coal-Fired Power Plants, Environmental

523   science & technology, 52, 2400-2408, 10.1021/acs.est.7b06209, 2018.

524   Liu, K., Wu, Q., Wang, L., Wang, S., Liu, T., Ding, D., Tang, Y., Li, G., Tian, H., Duan, L., Wang,

525   X., Fu, X., Feng, X., and Hao, J.: Measure-Specific Effectiveness of Air Pollution Control on China's

526   Atmospheric Mercury Concentration and Deposition during 2013-2017, Environmental science &

527   technology, 10.1021/acs.est.9b02428, 2019.

528   Lundberg, S. M. and Lee, S.-I.: A Unified Approach to Interpreting Model Predictions, 31st Annual

529   Conference on Neural Information Processing Systems (NIPS), Long Beach, CA, 2017

530   Dec 04-09, WOS:000452649404081, 2017.

531   Lundberg, S. M. and Lee, S. I.: A Unified Approach to Interpreting Model Predictions, 31st Annual

532   Conference on Neural Information Processing Systems (NIPS), Long Beach, CA, Dec 04-09,

533   WOS:000452649404081, 2017.

534   Lundberg, S. M., Erion, G., Chen, H., DeGrave, A., Prutkin, J. M., Nair, B., Katz, R., Himmelfarb,

535   J., Bansal, N., and Lee, S. I.: From Local Explanations to Global Understanding with Explainable AI for

536   Trees, Nat Mach Intell, 2, 56-67, 10.1038/s42256-019-0138-9, 2020.

537   Lundberg, S. M., Nair, B., Vavilala, M. S., Horibe, M., Eisses, M. J., Adams, T., Liston, D. E., Low,

538   D. K.-W., Newman, S.-F., Kim, J., and Lee, S.-I.: Explainable machine-learning predictions for the

539   prevention of hypoxaemia during surgery, Nature Biomedical Engineering, 2, 749-760, 10.1038/s41551-

540   018-0304-0, 2018.

541   Mangalathu, S., Hwang, S.-H., and Jeon, J.-S.: Failure mode and effects analysis of RC members

542   based on machine-learning-based SHapley Additive exPlanations (SHAP) approach, Engineering

543   Structures, 219, 110927, https://doi.org/10.1016/j.engstruct.2020.110927, 2020.

544   Mao, H., Cheng, I., and Zhang, L.: Current understanding of the driving mechanisms for

545   spatiotemporal variations of atmospheric speciated mercury: a review, Atmos. Chem. Phys., 16, 12897-

546   12924, 10.5194/acp-16-12897-2016, 2016.

547   Mazur, M., Mitchell, C. P. J., Eckley, C. S., Eggert, S. L., Kolka, R. K., Sebestyen, S. D., and Swain,

548   E. B.: Gaseous mercury fluxes from forest soils in response to forest harvesting intensity: A field

549   manipulation experiment, Sci. Total Environ., 496, 678-687, 10.1016/j.scitotenv.2014.06.058, 2014.

550   Moore, C. and Carpi, A.: Mechanisms of the emission of mercury from soil: Role of UV radiation,

551   J. Geophys. Res.-Atmos., 110, 10.1029/2004jd005567, 2005.

552   Obrist, D., Kirk, J. L., Zhang, L., Sunderland, E. M., Jiskra, M., and Selin, N. E.: A review of global

553   environmental mercury processes in response to human and natural perturbations: Changes of emissions,

554   climate, and land use, Ambio, 47, 116-140, 10.1007/s13280-017-1004-9, 2018.

555   Pacyna, E. G., Pacyna, J. M., Sundseth, K., Munthe, J., Kindbom, K., Wilson, S., Steenhuisen, F.,

556   and Maxson, P.: Global emission of mercury to the atmosphere from anthropogenic sources in 2005 and

557   projections to 2020, Atmospheric Environment, 44, 2487-2499, 10.1016/j.atmosenv.2009.06.009, 2010.

558   Pannu, R., Siciliano, S. D., and O'Driscoll, N. J.: Quantifying the effects of soil temperature,

559   moisture and sterilization on elemental mercury formation in boreal soils, Environmental Pollution, 193,

560   138-146, 10.1016/j.envpol.2014.06.023, 2014.

561   Poissant, L., Pilote, M., Constant, P., Beauvais, C., Zhang, H. H., and Xu, X. H.: Mercury gas

562   exchanges over selected bare soil and flooded sites in the bay St. Francois wetlands (Quebec, Canada),

563   Atmospheric Environment, 38, 4205-4214, 10.1016/j.atmosenv.2004.03.068, 2004.

564   Qi, Y., Li, Q., Karimian, H., and Liu, D.: A hybrid model for spatiotemporal forecasting of PM2.5

565   based on graph convolutional neural network and long short-term memory, The Science of the total

566   environment, 664, 1-10, 10.1016/j.scitotenv.2019.01.333, 2019.

567   Qin, X., Wang, X., Shi, Y., Yu, G., Zhao, N., Lin, Y., Fu, Q., Wang, D., Xie, Z., Deng, C., and Huang,

568   K.: Characteristics of atmospheric mercury in a suburban area of east China: sources, formation

569   mechanisms, and regional transport, Atmos. Chem. Phys., 19, 5923-5940, 10.5194/acp-19-5923-2019,

570   2019.

571   Qin, X., Zhou, S., Li, H., Wang, G., Wang, X., Fu, Q., Duan, Y., Lin, Y., Huo, J., Huang, K., and

572   Deng, C.: Simulation of Spatiotemporal Trends of Gaseous Elemental Mercury in the Yangtze River

573   Delta of Eastern China by an Artificial Neural Network, Environmental Science & Technology Letters,

574   10.1021/acs.estlett.1c01025, 2022.

575   Qin, X., Zhang, L., Wang, G., Wang, X., Fu, Q., Xu, J., Li, H., Chen, J., Zhao, Q., Lin, Y., Huo, J.,

576   Wang, F., Huang, K., and Deng, C.: Assessing contributions of natural surface and anthropogenic

577   emissions to atmospheric mercury in a fast-developing region of eastern China from 2015 to 2018, Atmos.

578   Chem. Phys., 20, 10985-10996, 10.5194/acp-20-10985-2020, 2020.

579   Selin, N. E., Jacob, D. J., Park, R. J., Yantosca, R. M., Strode, S., Jaegle, L., and Jaffe, D.: Chemical

580   cycling and deposition of atmospheric mercury: Global constraints from observations, J. Geophys. Res.-

581   Atmos., 112, 10.1029/2006jd007450, 2007.

582   Slemr, F., Brunke, E. G., Ebinghaus, R., and Kuss, J.: Worldwide trend of atmospheric mercury

583   since 1995, Atmospheric Chemistry and Physics, 11, 4779-4787, 10.5194/acp-11-4779-2011, 2011.

584   Soerensen, A. L., Jacob, D. J., Streets, D. G., Witt, M. L. I., Ebinghaus, R., Mason, R. P., Andersson,

585   M., and Sunderland, E. M.: Multi-decadal decline of mercury in the North Atlantic atmosphere explained

586   by changing subsurface seawater concentrations, Geophys. Res. Lett., 39, 10.1029/2012gl053736, 2012.

587   Stirnberg, R., Cermak, J., Kotthaus, S., Haeffelin, M., Andersen, H., Fuchs, J., Kim, M., Petit, J. E.,

588   and Favez, O.: Meteorology-driven variability of air pollution (PM1) revealed with explainable machine

589   learning, Atmos. Chem. Phys., 21, 3919-3948, 10.5194/acp-21-3919-2021, 2021.

590   Streets, D. G., Devane, M. K., Lu, Z. F., Bond, T. C., Sunderland, E. M., and Jacob, D. J.: All-Time

591   Releases of Mercury to the Atmosphere from Human Activities, Environmental science & technology,

592   45, 10485-10491, 10.1021/es202765m, 2011.

593   Streets, D. G., Horowitz, H. M., Jacob, D. J., Lu, Z., Levin, L., ter Schure, A. F. H., and Sunderland,

594   E. M.: Total Mercury Released to the Environment by Human Activities, Environmental science &

595   technology, 51, 5969-5977, 10.1021/acs.est.7b00451, 2017.

596   Tang, Y., Wang, S. X., Wu, Q. R., Liu, K. Y., Wang, L., Li, S., Gao, W., Zhang, L., Zheng, H. T., Li,

597   Z. J., and Hao, J. M.: Recent decrease trend of atmospheric mercury concentrations in East China: the

598   influence of anthropogenic emissions, Atmospheric Chemistry and Physics, 18, 8279-8291, 10.5194/acp-

599   18-8279-2018, 2018.

600   Vu, T. V., Shi, Z., Cheng, J., Zhang, Q., He, K., Wang, S., and Harrison, R. M.: Assessing the impact

601   of clean air action on air quality trends in Beijing using a machine learning technique, Atmos. Chem.

602   Phys., 19, 11303-11314, 10.5194/acp-19-11303-2019, 2019.

603   Wang, C., Feng, L., and Qi, Y.: Explainable deep learning predictions for illness risk of mental

604   disorders   in   Nanjing,   China,   Environmental   Research,   202,   111740,

605   https://doi.org/10.1016/j.envres.2021.111740, 2021.

606   Wang, G., Huang, K., Fu, Q., Chen, J., Huo, J., Zhao, Q., Duan, Y., Lin, Y., Yang, F., Zhang, W., Li,

607   H., Xu, J., Qin, X., Zhao, N., and Deng, C.: Response of PM2.5-bound elemental species to emission

608   variations and associated health risk assessment during the COVID-19 pandemic in a coastal megacity,

609   Journal of Environmental Sciences, 122, 115-127, 10.1016/j.jes.2021.10.005, 2022a.

610   Wang, G. C., Chen, J., Xu, J., Yun, L., Zhang, M. D., Li, H., Qin, X. F., Deng, C. R., Zheng, H. T.,

611   Gui, H. Q., Liu, J. G., and Huang, K.: Atmospheric Processing at the Sea-Land Interface Over the South

612   China Sea: Secondary Aerosol Formation, Aerosol Acidity, and Role of Sea Salts, J. Geophys. Res.-

613   Atmos., 127, 10.1029/2021jd036255, 2022b.

614   Wang, S. F., Feng, X. B., Qiu, G. L., Fu, X. W., and Wei, Z. Q.: Characteristics of mercury exchange

615   flux between soil and air in the heavily air-polluted area, eastern Guizhou, China, Atmospheric

616   Environment, 41, 5584-5594, 10.1016/j.atmosenv.2007.03.002, 2007.

617   Wang, X., Lin, C. J., and Feng, X.: Sensitivity analysis of an updated bidirectional air-surface

618   exchange model for elemental mercury vapor, Atmospheric Chemistry and Physics, 14, 6273-6287,

619   10.5194/acp-14-6273-2014, 2014.

620   Wanninkhof, R.: Relationship between wind speed and gas exchange over the ocean revisited,

621   Limnology and Oceanography-Methods, 12, 351-362, 10.4319/lom.2014.12.351, 2014.

622   Wen, M., Wu, Q., Li, G., Wang, S., Li, Z., Tang, Y., Xu, L., and Liu, T.: Impact of ultra-low emission

623   technology retrofit on the mercury emissions and cross-media transfer in coal-fired power plants, Journal

624   of Hazardous Materials, 396, 10.1016/j.jhazmat.2020.122729, 2020.

625   Wu, Q., Tang, Y., Wang, L., Wang, S., Han, D., Ouyang, D., Jiang, Y., Xu, P., Xue, Z., and Hu, J.:

626   Impact of emission reductions and meteorology changes on atmospheric mercury concentrations during

627   the   COVID-19   lockdown,   The   Science   of   the   total   environment,   750,   142323,

628   10.1016/j.scitotenv.2020.142323, 2021.

629   Wu, Q. R., Wang, S. X., Liu, K. Y., Li, G. L., and Hao, J. M.: Emission-Limit-Oriented Strategy To

630   Control Atmospheric Mercury Emissions in Coal-Fired Power Plants toward the Implementation of the

631   Minamata Convention, Environmental science & technology, 52, 11087-11093, 10.1021/acs.est.8b02250,

632   2018.

633   Wu, Q. R., Wang, S. X., Li, G. L., Liang, S., Lin, C. J., Wang, Y. F., Cai, S. Y., Liu, K. Y., and Hao,

634   J. M.: Temporal Trend and Spatial Distribution of Speciated Atmospheric Mercury Emissions in China

635   During 1978-2014, Environmental science & technology, 50, 13428-13435, 10.1021/acs.est.6b04308,

636   2016.

637   Xin, M. and Gustin, M. S.: Gaseous elemental mercury exchange with low mercury containing soils:

638   Investigation of controlling factors, Appl. Geochem., 22, 1451-1466, 10.1016/j.apgeochem.2007.02.006,

639   2007.

640   Xu, J., Wang, Q. Z., Deng, C. R., McNeill, V. F., Fankhauser, A., Wang, F. W., Zheng, X. J., Shen,

641   J. D., Huang, K., and Zhuang, G. S.: Insights into the characteristics and sources of primary and

642   secondary organic carbon: High time resolution observation in urban Shanghai, Environmental Pollution,

643   233, 1177-1187, 10.1016/j.envpol.2017.10.003, 2018.

644   Xu, J., Chen, J., Shi, Y. J., Zhao, N., Qin, X. F., Yu, G. Y., Liu, J. M., Lin, Y. F., Fu, Q. Y., Weber, R.

645   J., Lee, S. H., Deng, C. R., and Huang, K.: First Continuous Measurement of Gaseous and Particulate

646   Formic Acid in a Suburban Area of East China: Seasonality and Gas-Particle Partitioning, Acs Earth and

647   Space Chemistry, 4, 157-167, 10.1021/acsearthspacechem.9b00210, 2020.

648   Xu, X., Liao, Y., Cheng, I., and Zhang, L.: Potential sources and processes affecting speciated

649   atmospheric mercury at Kejimkujik National Park, Canada: comparison of receptor models and data

650   treatment methods, Atmospheric Chemistry and Physics, 17, 1381-1400, 10.5194/acp-17-1381-2017,

651   2017.

652   Yang, J., Wen, Y., Wang, Y., Zhang, S., Pinto, J. P., Pennington, E. A., Wang, Z., Wu, Y., Sander, S.

653   P., Jiang, J. H., Hao, J., Yung, Y. L., and Seinfeld, J. H.: From COVID-19 to future electrification:

654   Assessing traffic impacts on air quality by a machine-learning model, Proc Natl Acad Sci U S A, 118,

655   10.1073/pnas.2102705118, 2021.

656   Yin, X., Kang, S., de Foy, B., Ma, Y., Tong, Y., Zhang, W., Wang, X., Zhang, G., and Zhang, Q.:

657   Multi-year monitoring of atmospheric total gaseous mercury at a remote high-altitude site (Nam Co,

658   4730 m a.s.l.) in the inland Tibetan Plateau region, Atmospheric Chemistry and Physics, 18, 10557-10574,

659   10.5194/acp-18-10557-2018, 2018.

660   Zhang, L., Wang, S., Wu, Q., Wang, F., Lin, C. J., Zhang, L., Hui, M., Yang, M., Su, H., and Hao,

661   J.: Mercury transformation and speciation in flue gases from anthropogenic emission sources: a critical

662   review, Atmos. Chem. Phys., 16, 2417-2433, 10.5194/acp-16-2417-2016, 2016a.

663   Zhang, Y., Jacob, D. J., Horowitz, H. M., Chen, L., Amos, H. M., Krabbenhoft, D. P., Slemr, F., St

664   Louis, V. L., and Sunderland, E. M.: Observed decrease in atmospheric mercury explained by global

665   decline in anthropogenic emissions, Proc Natl Acad Sci U S A, 113, 526-531, 10.1073/pnas.1516312113,

666   2016b.

667   Zheng, B., Tong, D., Li, M., Liu, F., Hong, C., Geng, G., Li, H., Li, X., Peng, L., Qi, J., Yan, L.,

668   Zhang, Y., Zhao, H., Zheng, Y., He, K., and Zhang, Q.: Trends in China's anthropogenic emissions since

669   2010 as the consequence of clean air actions, Atmospheric Chemistry and Physics, 18, 14095-14111,

670   10.5194/acp-18-14095-2018, 2018.

671   Zhong, S., Zhang, K., Wang, D., and Zhang, H.: Shedding light on "Black Box" machine learning

672   models for predicting the reactivity of HO radicals toward organic compounds, Chemical Engineering

673   Journal, 405, 126627, https://doi.org/10.1016/j.cej.2020.126627, 2021.

674   Zhu, W., Lin, C. J., Wang, X., Sommar, J., Fu, X., and Feng, X.: Global observations and modeling

675   of atmosphere–surface exchange of elemental mercury: a critical review, Atmos. Chem. Phys., 16, 4451-

676   4480, 10.5194/acp-16-4451-2016, 2016.

677   Zhu, W., Sommar, J., Li, Z., Feng, X., Lin, C.-J., and Li, G.: Highly elevated emission of mercury

678   vapor due to the spontaneous combustion of refuse in a landfill, Atmospheric Environment, 79, 540-545,

679   10.1016/j.atmosenv.2013.07.016, 2013.

680